Spatiotemporal control of the bacteria to express interferon-γ by focused ultrasound for tumor immunotherapy

Yuhao Chen
The First Affiliated Hospital, Medical Imaging Centre, Hengyang Medical School, University of South China

Meng Du
The First Affiliated Hospital, Medical Imaging Centre, Hengyang Medical School, University of South China

Zhen Yuan
University of Macau

Fei Yan
Shenzhen Institutes of Advanced Technology

Zhiyi Chen (zhiyi_chen@usc.edu.cn)
The First Affiliated Hospital, Medical Imaging Centre, Hengyang Medical School, University of South China

---

Article

Keywords: Bacterium, Tumor therapy, Ultrasound, Interferon-γ, Immunotherapy, Inducible gene expression

Posted Date: August 16th, 2021

DOI: https://doi.org/10.21203/rs.3.rs-788033/v1

Version of Record: A version of this preprint was published at Nature Communications on August 2nd, 2022. See the published version at https://doi.org/10.1038/s41467-022-31932-x.

Abstract

Bacteria-based tumor therapy has recently attracted wide attentions due to its unique capability in targeting tumors and preferentially colonizing the core area of the tumor. Various therapeutic genes were also harbored into these engineering bacteria to enhance their anti-tumor efficacy. However, it is difficult to spatiotemporally control the expression of these inserted genes in the tumor site. Here, we engineered an ultrasound-responsive bacterium (URB) which can induce the expression of exogenous genes in an ultrasound-controllable manner. Owing to the advantage of ultrasound in the tissue penetration, energy focusing into heating, an acoustic remote control of bacterial gene expression can be realized by designing a temperature-actuated genetic switch. Cytokine interferon-γ (IFN-γ), an important immune regulatory molecule that plays a significant role in tumor immunotherapy, was used to test the system. Our results showed a brief hyperthermia by focused ultrasound successfully induced the expression of IFN-γ gene, significantly improving anti-tumor efficacy of URB *in vitro* and *in vivo*. Our study provided a novel strategy for bacteria-mediated tumor immunotherapy.

1. Introduction

Bacteria-mediated tumor therapy has recently attracted wide attentions as tumor-targeting drug delivery system or as anti-tumor live agents by themselves because of the characteristic of solid tumors, such as hypoxic, immunosuppressive, and biochemically unique microenvironment[1–3]. Compared to other drug delivery carriers, bacteria-based delivery system has many advantages, including: 1) bacteria could actively target hypoxic, eutrophic, and immunosuppressive tumor microenvironment, breaking through the resistance of tumor blood vessel and the high interstitial pressure and proliferating in the tumor[4, 5]. This occurs primarily due to reduced immune surveillance along with the ability of bacteria to grow within the hypoxic and necrotic tumor core. Because bacteria are both inherently present and selectively grow within tumors, they provide a natural platform for the development of programmable therapeutic delivery vehicles[6, 7]. 2) Also, some engineered bacteria can carry therapeutic genes such as encoding PD-L1 single chain antibody or TNF-a through inserting them into prokaryotic expression vector, which not only entrusts them with hereditability along with their hosts, but also makes it possible to combine multiple genes for maximize their anti-tumor efficacy[8–11]. 3) More importantly, the introduction of synthetic biology technologies into these engineered bacteria, such as promoter engineering, smart genetic circuits greatly improved their ability to sense and response to disease states of inflammation, infection, and to control bacteria growth and gene expression, largely improving their selective colonization of tumors and convenient opportunity for tumor drug delivery[12–14].

To date, many techniques have been developed for studying inducible gene expression in bacteria, including chemical induction, physical stimulation and biological methods[15, 16]. Conventionally, systemically administered chemical inducers are not specific to a particular anatomical site. The tumor microenvironment with high interstitial fluid pressure makes it difficult for chemical inducers to accumulate to the ideal concentration, while increasing their doses may possibly bring with potential side

effects[17–19]. Some biological methods such as the bacterial quorum sensing systems can adjust gene expression in concert with their population size, making it possible to initiate therapeutic gene expression only when their population density reaches a threshold level[14, 16]. But it is difficult for the biological methods to precisely model gene expression in a spatiotemporally controllable manner, especially in live animals. Physical induction approaches, such as ray irradiation and light stimulation, provide high spatiotemporal precision. But the former is ionizing which may cause damage to the normal tissues in the irradiation path[20], and the latter is limited by the poor penetration into the deep-seated tumors[21]. In contrast, ultrasound has many advantages in noninvasiveness, safety and tissue penetration[22–24]. Importantly, thanks to the thermal effects, the beam waves excited by ultrasound can be focused into the deep tissues and precisely and locally elevate the temperature of irradiated region through converting the mechanical energy into heat energy. Thus, it may provide an ideal remote regulation of bacterial gene expression when combining with temperature-based gene control elements[25]. Our previous studies have used ultrasound as a trigger source for drug release in temperature-sensitive liposomes to achieve targeted controlled release of drugs at tumor sites[26].

The leftward (PL) and rightward (PR) phage lambda promoters are strong and finely temperature-regulated promoter elements, which have been employed for the production of many recombinant proteins and peptides in some widely used prokaryotic expression vectors[27]. Transcription from either promoter or both in tandem would be repressed in prokaryotic cells growing at low temperature (28–30°C) by the thermolabile cI857 repressor expressed from the same vector, while a temperature shift to 42–45°C would rapidly result in the inactivation of cI857 repressor, making it possible to transcribe the appropriately inserted genes under the promoters and to overproduce their encoded recombinant proteins. By using of the thermo-regulated expression system, many heterologous recombinant proteins and peptides have been successfully induced and produced, avoiding the use of special media, toxic or expensive chemical inducers[28, 29]. Therefore, we developed an ultrasound-responsive bacterium (URB) which can spatiotemporally control the gene expression by focused ultrasound-induced hyperthermia in this study. In this system, the IFN-γ or mCherry genes were inserted into the multiple clone site under PL and PR tandem promoter and further introduced them into the *E. coli* MG1655 that can accumulate in the hypoxic and necrotic areas of tumors (Fig. 1). Upon their delivery into the tumors, focused ultrasound was used to irradiate and heat these bacteria, triggering the expression of IFN-γ gene and activating the anti-tumor immune response. The production and secretion of IFN-γ not only can promote the apoptosis of cancer cells, but also induce the macrophage polarization from M2 to M1 phonotype, further activating $CD4^+$ and $CD8^+$ T cells to kill the cancer cells (Fig. 1, right panel). Interestingly, plasma IFN-γ secreting from URB also can polarize the macrophages in murine spleen, enhancing their antigen presenting effects and producing more $CD4^+$ and $CD8^+$ T cells to inhibit the tumor metastasis and distant tumor growth (Fig. 1, left panel). Thus, a high spatiotemporal controllable gene expression strategy in deep tissues was developed through the remote noninvasive ultrasound in this work.

2. Result And Discussion

2.1 Hyperthermia and ultrasound triggered gene expression of URB

We first constructed the prokaryotic expression plasmid harboring temperature-actuated therapeutic circuit which carries murine IFN-γ gene or mCherry fluorescent reporter under the pR-pL tandem promoter (Fig. 2a). Then the recombinant plasmid was introduced into *E. coli* MG1655 (a non-pathogenic bacterium) to produce ultrasound responsive bacteria (URB). Incubation of the engineered bacteria harboring mCherry gene at 37°C did not produce any fluorescence signals, showing the suppressed expression of mCherry fluorescent gene at 37°C. In contrast, strong red fluorescent signals could be observed at 6 h after the bacterium incubation temperature rose to 45°C, revealing that TcI repression was relieved to initiate the mCherry gene expression (Fig. 2b). Prolonging the incubation time at 45°C from 5 min to 25 min increased the fluorescent signal intensities, which confirmed the controllability of thermal logic circuits of URB (Fig. 2c). To develop a noninvasive remote control of bacterial gene circuits by focused ultrasound, we optimized a series of acoustic parameters including acoustic energies, irradiation duration time at on/off state. Results showed that the parameters at 4.93 MPa acoustic pressure, 3 s ON and 5 s OFF irradiation time could keep the irradiated bacterium solution at 45°C constant temperature (Fig. 2d). After the ultrasound irradiation, URB could successfully express mCherry fluorescent protein and the fluorescence signal intensity increased gradually along with time (Fig. 2e). To elucidate the remote controllability of bacterial gene expression, we inserted a tube of bacteria into an agar phantom with or without acoustic exposure for 30 min at the optimal ultrasound parameters. Figure 2f showed the fluorescence signals only appeared in the sample received with ultrasound irradiation, but not in these bacteria that did not receive with ultrasound exposure. In addition to controlling the temperature of the bacterial solution *in vitro*, the temperature of the local tissue of mice could also be increased to 45°C by adjusting the appropriate ultrasonic parameters (Figure S1). *In vivo* animal experiment further revealed that the liver of mouse administrated intravenously with URB could emit the strong fluorescence signals after ultrasound irradiation at the above optimized acoustic parameters. By contrast, the livers from the non-irradiated control mice or the incubator-heating mice at 45°C did just emit weak background fluorescence signals (Fig. 2g-h). These results showed that ultrasound can function as a remote tool to regulate the gene expression of bacteria when they harbor some temperature-based gene control elements *in vitro* and *in vivo*. Previous report synthesized a thermosensitive therapeutic bacterium and triggered the in-situ expression of TNF-α of bacteria by near-infrared light irradiation[21]. However, it is difficult to act on deep tumor tissues in live animals because of weak penetration of near-infrared light. Compared to near-infrared light, ultrasound could irradiate the deeper tissue such as liver, which may be more suitable for the induction of bacteria located in the deep tumor.

2.2 *In vitro* treatment experiment of URB-mediated tumor immunotherapy

Next, we engineered one therapeutic URB by displacing the fluorescent mCherry gene with murine IFN-γ gene in the thermal logic circuits. Agarose gel electrophoresis confirmed the presence of IFN-γ gene

fragment in the plasmid (Figure S2). SDS-PAGE gel electrophoresis analysis revealed that IFN-γ proteins appeared only in the lysate of bacteria incubated at 45°C for 30 min, but not in the lysate of bacteria incubated at 37°C, confirming the production of therapeutic IFN-γ after thermal treatment (Fig. 3a). Moreover, the therapeutic IFN-γ protein expressed from URB was water-soluble (Figure S3). Prolonging the incubation and ultrasound irradiation time at 45°C from 20 min to 80 min increased the expression level of IFN-γ proteins, showing an excellent time-dependent correlation (Fig. 3b-c). These results showed the designed therapeutic logic circuit can be strictly controlled and tuned by heating and ultrasound stimulation and their exposure duration, which is important for many therapeutic factors to execute their anti-tumor effects. To test whether the IFN-γ proteins could be secreted from their host bacteria to kill tumor cells, the calcium AM/PI staining assay was used to 4T1 breast cancer cells which were incubated with different concentrations of IFN-γ proteins from 50–150 pg/ml in the bacterial supernatant. Obviously, almost all the cells showed green fluorescence in the blank group, showing no dead cells. With the increase of IFN-γ proteins, the proportion of living cells (green fluorescence) decreased gradually, while the proportion of dead cells (red fluorescence) increased gradually (Fig. 3d). Quantitative analysis by CCK-8 kits revealed that the cell viability was 33.13 ± 16.28 %, 38.93 ± 4.72 %, 47.02 ± 72.62 %, 63.09 ± 4.14 % or 68.50 ± 3.11 % for 150 pg/ml, 125 pg/ml, 100 pg/ml, 75 pg/ml or 50 pg/ml IFN-γ proteins in the bacterial supernatant, respectively. It was significantly lower than these cells incubated with the equivalent supernatant from non-induced bacteria (Fig. 3e).

IFN-γ can exert its cytotoxicity and immunoregulatory effects by activating Janus kinase 1 (JAK1) and signal transducers and activators of transcription1 (STAT1) signaling pathways[30–32]. The effect of IFN-γ expressed from URB on macrophage immune activation was further examined *in vitro*. The RAW 264.7 macrophages were incubated with IFN-γ expressed by bacteria for about 8 h, revealing a similar effect as the traditional IFN-γ in promoting the generation of proinflammatory M1 phenotype macrophages, with about 71.6% of macrophages staining positive for CD86 and 85.4% for CD80 at 150 pg/mL bacterial IFN-γ (Fig. 3h). Also, the significantly decreased expression of M2 phenotype marker CD206 could be observed on the macrophages, confirming that IFN-γ released from the URB can induce the macrophage polarization from M2 to M1 phonotype. Meanwhile, the bacterial IFN-γ also triggered to produce higher level of NO in the macrophages in comparison with the control group (Fig. 3f). Furthermore, we detected the tumor cell killing efficacy of these activated macrophages stimulated by different concentrations of bacterial IFN-γ, finding that higher concentrations of IFN-γ were used to stimulate macrophages, stronger cytotoxicity these activated macrophages would be (Fig. 3g). Together, the above results demonstrated that the IFN-γ produced from bacteria could effectively activate macrophages.

3.3 Tumor targeting of URB

In order to detect the tumor-targeting property of these engineered bacteria, the DiR-labelled live URB or dead URB treated with 65°C for 30 min were injected intravenously into the 4T1 tumor-bearing mice and imaged by an IVIS Spectrum imaging system at different time. As shown in Fig. 4a, the live URB revealed the efficient tumor-homing ability in the 4T1 tumor, emitting strong fluorescence at 6 h after injection. Increasing fluorescence at the tumor site was observed along with time from the mice received live DiR-

labelled URB administration, but not from the control mice injected with the dead URB. 48 h after administration, mice were euthanized to analyze the fluorescence signals in various organs (Fig. 4b). According to the results, It was showed that the distribution of dead URBs are mainly in liver and spleen. On the contrary, the accumulation of the live URBs was higher in the tumor site, and less in the liver than the control group. The quantitative analysis revealed a five-fold increase of relative fluorescence intensity in the tumor of live URB group compared with dead URB, which is in consistent with the results of *in vivo* fluorescence imaging (Fig. 4c).

Subsequently, the targeting efficiency of DiR-labelled URBs to the tumors was determined by fluorescence microscope observation. As Fig. 4d showed, the red fluorescence signal, which represent the distribution of DiR-labelled live URB, mainly appeared in the tumor tissues but not in the heart, kidney and lung, and a bit in the liver and spleen. By contrast, only a little of red fluorescence could be observed in the tumor for DiR-labelled dead URB. Interestingly, the red fluorescence of DiR-labelled live URB were largely distributed in the center of tumors which represents the hypoxic and necrotic region due to the insufficient nutrient supply. Different from the live URB, the dead URB mainly appeared in the peritumoral zone. These results illustrated that the live URBs rather than the dead URBs could be efficiently accumulated in the tumor site and penetrated the tumor hypoxic and necrotic region. It may be the chemoreceptors on the surface of *E. coli* sense the nutrient-rich and low-oxygen tumor microenvironment, promoting them to actively migrate in the tumor region[33, 34]. In order to further explore the behaviors of these engineered URB after intravenous injection, 4T1-bearing mice received URB at the dose of 1×10^7 colony-forming units (CFU) per mouse via intravenous injection and then sacrificed at 1, 2, 7, 14, and 21 days after injection. Various organs and tumor were collected, homogenized, serially diluted (10-10000 fold), and incubated on Luria-Bertani (LB) plates containing 100 μg/ml ampicillin. The data colony counts in each plate revealed that URB were gradually eliminated from heart, liver, spleen, lung and kidney (Fig. 4, e and f). However, the colony counts of tumors showed exponential growth along with the time, achieving the peak value after 7 days and then decreasing gradually (Fig. 4, e and g). There was not bacterial colony formation from any tissue homogenates when the dead URB were used for intravenous injection into these mice. Collectively, these results provided evidence for their capability of the engineered bacteria to home, penetrate and colonize in the tumors, attributing to the hypoxic, immunosuppressive, and biochemically unique tumor microenvironment[35–37].

3.4 *In vivo* experiment of URB-mediated tumor immunotherapy

To evaluate the anti-tumor effect of URBs combined with focused ultrasound *in vivo*, unilateral 4T1 tumor-bearing mice model were treated following the therapeutic schedule in Fig. 5a. The mice were randomly separated into six groups and treated with saline (control), ultrasound alone (US), MG1655 *E. coli* harboring without the circuit (*E. coli*), URB harboring the circuit (URB), *E. coli* + ultrasound (*E. coli* + US) or URB + US group, respectively. 48 h after intravenous injection, Ultrasound irradiation was performed to trigger the expression of IFN-γ. The treatment procedure was repeated seven days later. As

shown in Fig. 5b-d, the volume of tumors in each group was similar on the day 1. However, URB + US group exhibited the strongest tumor inhibitory effect against tumor growth and the longest postsurgical survival time. The average tumor volume of the mice treated with URB + US was less than 250 mm^3, whereas that of other treated groups are more than 1000 mm^3.The median survival time of mice in URB + US group increases to 57 days compared with 42 days for control group, which proved that application of URB combined with ultrasound irradiation could improve survival rate significantly. Compared with other groups, It was showed that apparent damages were observed on the tumor cells after the treatment of URB + US (Fig. 5e, upper row). The maximum degree of cell apoptosis was also found by terminal deoxynucleotidyl transferase-mediated dUTP nick end labeling (TUNEL) assay (Fig. 5e, middle row). Moreover, URB + US showed much less expression of Ki67 in immunofluorescence staining (Fig. 5e, bottom row), demonstrating significant reduced tumor proliferation potentials.

Since IFN-γ can induce polarization of M1 macrophages[38], we further explored whether the treatment activated the intratumoral immune response. Flow cytometry for the polarization of tumor-associated macrophages (TAMs) demonstrated $CD80^+$ macrophages greatly improved and $CD206^+$ macrophages significantly decreased in the tumors treated with URB + US in comparison with control, only US and only URB groups, indicating that URB + US treatment could effectively promote the polarization of TAMs from M2 phenotype towards M1 phenotype (Fig. 5f). The polarization of TAMs markedly increased $CD8^+$ T cells (Fig. 5g). Meanwhile, significantly higher IFN-γ and TNF-α levels but less IL-10 levels could be detected at 1, 3 and 5 days after URB + US treatment. Thus, our data suggested that URB combined with ultrasound could effectively activate antitumor immunity through inducing the expression of IFN-γ. Some previous studies have used IFN-γ for tumor treatment and found that the infiltration of lymphocytes such as $CD4^+$ T cells, $CD8^+$ T cells, and macrophages in the tumor microenvironment increased significantly[39]. The significantly reduced ability of TAM to produce arginase-1 and iNOS was also demonstrated after IFN-γ treatment[40]. All these data suggested that IFN-γ can promote M1 macrophages in the tumor microenvironment, thereby improving the efficacy of tumor immunotherapy.

3.5 *In vivo* experiment of URB-mediated tumor immunotherapy

Since the antitumor immunity of URB could be effectively activate by ultrasound *in vitro*, we next wander whether the immune response triggered by URB combined with ultrasound can inhibit the growth of distant tumors. Bilateral 4T1 tumor-bearing mice model were established to explore the treatment-elicited abscopal (left) therapeutic effect by treating the primary (right) tumor. As depicted in Fig. 6a, 4T1 cancer cells were inoculated at day − 10 (right) and day − 7 (left), respectively. A week later when the right flank tumors were about 100 mm^3 (day 0), the engineered URB at 10^7 CFU were systemic administrated by tail vein and followed by ultrasound irradiation at two days later (day 2). As expected, significant antitumor effects were observed in the primary tumors received with ultrasound irradiation and URB administration (Fig. 6b-c). Interestingly, the distant tumors from URB + US group were also greatly inhibited in comparison with control, US, *E. coli*, URB, *E. coli* + US groups (Fig. 6b and d). The survival rate of the mice

treated with URB + US was greatly improved, with more than 80% of them still alive on 60th day post the tumor inoculation (Fig. 6e). Notably, only very few metastatic foci were observed in the lungs of mice treated with URB + US (Fig. 6e–g), suggesting effective inhibition of lung metastasis. In addition, we also demonstrated that systemic administration of URB did not cause severe side effects to mice by body weight monitoring (Figure S4). All of these data indicated URB + US resulted in a robust anti-tumor immune effect to protect mice from distant tumors and metastasis.

To understand the mechanism of the antitumor systemic effects triggered by URB plus ultrasound, immune cells in the spleen were assessed on the 7th day after the first treatment by bilaterally 4T1 cancer model. The percentage of M1 phenotype macrophages ($CD80^+$) and M2 phenotype macrophages ($CD206^+$) in spleens was evaluated. The results showed that the proportion of $CD80^+$ macrophages in the URB + US group was 18.9 ± 3.38%, with a significantly increase compared with saline control group (8.78 ± 2.66%). In contrast, the proportion of $CD206^+$ macrophages in spleen were significantly decreased to 19.5 ± 3.02% (Fig. 6i). Specifically, the percentage of $CD8^+$ T cell in the URB + US group occupied 34.7 ± 4.49% with an increase by nearly 3.7 times in comparison with the control group (Fig. 6j). There was a statistically increase in the percentage of $CD4^+$ T cell in the spleen treated with URB + US group (Figure S7 a), while the proportion of DC and NK cell was slightly increased in the combined treatment (Figure S7 b-c). The antitumor systemic immune response elicited by URB + US was further verified by the cytokine detection. It has been found that URB + US significantly promoted the IFN-γ and TNF-α level in blood (Fig. 6k-l). These results indicated that the URB + US combined therapy could trigger the systematic antitumor immunity to inhibit the distant tumor growth and metastasis[41–43].

In order to further explore the biosafety of this therapeutic strategy, the changes of mice weight and major organs histopathologic features was evaluated. It is found that no abnormal weight changes of mice were found in the different treatment (Figure S5), demonstrating the good biosafety of the URB-mediated immunotherapy. In addition, cell damage was not observed in the H□E staining slices of various organs of different group mice (Figure S8). The blood biochemistry and blood routine were recorded that all the indexes of the URB + US group were not significantly different from those of the other group (Table S1-S2). Because URB had less accumulation in normal tissues such as organs and blood. With the elimination of the immune system, URB has the short half-life in major organs. Previous studies used a similar bacteria strain to our study, *E. coli* MG1655, and confirmed that the strain was safe and did not affect the homeostasis of the body[21]. Together, the results demonstrated that the novel targeted therapeutic strategy integrating URB with ultrasound holds great potential in cancer immunotherapy.

3. Conclusion

In summary, we have developed a new genetically engineered bacterium (URB) with ultrasound responsiveness and applied them to tumor immunotherapy in an ultrasound-controllable gene expression manner. Our study reveals the URB had good tumor-targeting capabilities and reliable tumor-suppressive effects upon their exposure to ultrasound for expressing therapeutic genes. This approach allows to

effectively enhance the targeting and safety of therapeutic protein delivery, which was expected to be extended to bacteria-mediated tumor treatment and had potential value in clinical applications. The ultrasound combined with URB is likely to enable the development of a controllable, noninvasive tumor treatment strategy that would greatly promote the research development in the field of bacteria-mediated immunotherapy. In conclusion, we developed a high spatiotemporally controllable gene expression strategy in deep tissues through the focused ultrasound.

4. Materials And Methods

4.1 Materials

The IFN-γ gene sequence was obtained from GenBank and synthesized by Sangon bioengineering Co. (Shanghai, China). The pBV220 plasmid was purchased from Miaoling Bioscience & Technology Co. (Wuhan, China). *E. coli* DH5α strain and *E. coli* MG1655 strain were purchased from Angyubio Biotechnology Co. (Shanghai, China). The mouse breast cancer cells (4T1) were obtained from American Type Culture Collection. Dulbecco's modified Eagle's medium (DMEM) culture medium, fetal bovine serum (FBS), penicillin and streptomycin solution, trypsin containing 0.25% EDTA were purchased from Gibco (USA). 1,1-dioctadecyl-3,3,3,3-tetramethylindotricarbocyanine iodide (DiR), live & dead cell viability detection kit and CCK-8 assay kit were obtained from Beyotime Biotechnology Co. (Shanghai, China). Murine IFN-γ, TNF-α and IL-10 enzyme-linked immunosorbent assay (ELISA) kits were obtained from Dakewe Bio-engineering Co. (Shenzhen, China). The antibodies used for flow cytometry were the following: CD11b-FITC, CD206-PE, CD86-Cy5.5, CD80-APC, CD45-APC 750, CD3-APC, CD4-Alexa Flour 700, CD8-FITC, obtained from Biolegend (USA).

4.2 Preparation of ultrasound-responsive bacteria

The IFN-γ gene fragment was inserted into a pBV220 plasmid through EcoRI and SalI enzyme digestion and ligation reactions to generate the IFN-γ-expressed thermosensitive plasmid (pBV220-IFN-γ). The recombinant plasmid was transformed into *E. coli* DH5α competent cells. The construction of pBV220-IFN-γ plasmid was confirmed by DNA sequencing. Also, the mCherry-expressed thermosensitive control plasmid (pBV220-mCherry) was constructed to facilitate the detection of gene expression. The pBV220-IFN-γ or pBV220-mCherry plasmids were transformed to the *E. coli* MG1655 strain to obtain ultrasound-responsive bacteria (URB). The resulting URBs were plated on LB solid plate and then incubated at 37℃ for 12 h. URB colonies were picked out and amplified in LB liquid medium at 30℃, 220 rpm overnight. Afterward, the URB liquid was diluted by 100-folds into fresh LB medium and further grown to the OD_{600} = 0.4–0.6 for further experiments.

4.3 Thermal-induced and ultrasound-induced mCherry gene expression

The URB transformed with pBV220-mCherry plasmid were incubated at 37℃ or 45℃ for a given time and further incubation for 6 h at 37℃. The IVIS Spectrum was used to detect the fluorescence signal of

bacteria. To test the feasibility of ultrasound-induced mCherry gene expression, the URB was added to a 96-well plate (200 μl each well). Ultrasound with acoustic pressure of 2.82 MPa, 3.17 MPa, 3.52 MPa, 3.88 MPa, 4.22 MPa and 4.93 MPa were used to generate heating to induce gene expression. Other ultrasound parameters were as follows: frequency = 960 Hz, pulse period = 150 ms, pulse width = 100 ms. The temperature was monitored by an infrared thermal imager. The On/Off ultrasound irradiation procedure was adjusted to keep the temperature constant. After ultrasound irradiation, the fluorescence signal of bacterial solution was observed at different time points by IVIS Spectrum. To examine the penetration of the ultrasonic stimulation, 1% agar phantom was made and inserted a tube filled with URB, keeping the URB 10 cm away from the transducer. Then the tube was irradiated by ultrasound through the agar gel for 30 min. The fluorescence signal of URB was detected by IVIS Spectrum. As the detection of gene expression, 5×10^7 CFU / ml URB were injected into the Balb/c mice via the tail vein and ultrasound was applied at 3.52 MPa acoustic pressure for 30 min, and the fluorescence signal of mice and the major organs were detected by IVIS system after 6 h (Excitation wavelength: 745 nm, emission band pass: 800 nm). As a control, the mice in heat group were placed in a 45°C incubator for 30 min.

4.4 Thermal-induced and ultrasound-induced IFN-γ gene expression

The URB transformed with pBV220-IFN-γ plasmid was cultured to OD_{600} 0.4 ~ 0.6 in 30℃ moved to 37℃ or 45℃ for a given time. After that, the bacteria total proteins were analyzed using SDS-PAGE to detect the expression of IFN-γ. To determine the expression level of IFN-γ induced by ultrasound, the URB at OD_{600} 0.4 ~ 0.6 was added to a 96-well plate and exposed to ultrasound (acoustic pressure = 3.52 MPa) for 20 min to 80 min. and the murine IFN-γ ELISA kit was used to quantitatively analyze the concentration of IFN-γ in bacterial culture medium.

4.5 Cell cytotoxicity of IFN-γ expressed by URB

Calcein AM/PI staining was used to detect the 4T1 breast cancer cell viability after IFN-γ treatment. Briefly, the breast cancer 4T1 cells were seeded into a 96-well plate (1×10^4 cells per well), and then incubated in 100 μL DMEM medium containing 10% FBS for a 12 h in an incubator. Then 100 μL fresh DMEM medium containing bacterial culture medium with 50 pg/mL to 150 pg/mL concentrations of IFN-γ were added into the well and incubated for 6 h. After washed with PBS for three times, the 4T1 cells were incubated with 100 μL Calcein AM/PI staining solution and incubated for 30 min in the incubator. The fluorescence microscope was used to observe the fluorescent signal of tumor cells. CCK-8 assay was also used to detect the cell cytotoxicity of IFN-γ expressed by URB according to the production illustration.

4.6 Immunological activity of IFN-γ expressed by URB

The immunological activity of IFN-γ expressed by URB was evaluated by macrophages activation. RAW 264.7 macrophages were seeded into a 96-well plate (8×10^3 cells per well), and then incubated in 100 μL DMEM medium containing 10% FBS for a 12 h in an incubator. Then 100 μL fresh DMEM medium containing bacterial culture medium with 50 pg/mL to 150 pg/mL concentrations of IFN-γ were added

into the well and incubated for 48 h. After that, The NO detection kit was used to detect the NO level in macrophage culture medium. To detect the surface markers of macrophages, the treated RAW 264.7 macrophages were collected and washed with pre-cooled PBS for three times. Antibodies including perCy5.5-labeled CD86, APC -labeled CD80 and PE-labeled CD206 were used to analyze these markers by flow cytometry. Moreover, the activated RAW 264.7 macrophages were collected and used to co-incubate with tumor cells in a MOI ratio of 5:1 in 96-well plate for 12 h, and the tumor killing activity was evaluated with CCK-8 kit.

4.7 Breast cancer model

Female BALB/c mice were purchased from Vital River Laboratory Animal Technology Co. (Beijing, China). Animal experiments were approved by the Institutional Animal Care and Use Committee (IACUC) of the Animal Experiment Center of Shenzhen Institutes of Advanced Technology, Chinese Academy of Sciences. The female BALB/c mice (4–6 weeks old) were used to establish xenograft tumor model. 1×10^7 4T1 breast cancer cells in 100 μl cell suspension were injected subcutaneously into the right thigh of the mice. The tumor volume was measured every 2 days after tumor implantation, and the treatment procedure was performed when the mice tumor volume reached to 100 mm^3.

4.8 Tumor targeting of URB

The concentration of URB was adjusted to 1×10^8 CFU / ml URB. DiR dye was added to the URB solution (30 μl/mL) and incubated at 37℃ for 45 min. The bacteria solution was washed with PBS until the supernatant was clear. The bacteria were injected into the tumor-bearing mice via the tail vein (1×10^7 CFU per mouse) (n = 4). At the given time points, the mice were imaged by IVIS system (PekinEmer) to evaluate the biodistribution and tumor accumulation of bacteria. 48 h after the intravenous injection, tumor-bearing mice were sacrificed and the organs including heart, lung, liver, kidney, spleen and tumor were collected for the *ex vivo* fluorescence imaging. As the control, the dead URB were treated at 65 ℃ for 30 min. To evaluate the number of URB in each organ (CFU per gram of tissue), different time after administration with URB at 1 day, 2 day, 7 day, 14 day and 21 day, organs of mice including heart, liver, spleen, lung, kidney and tumor were harvested, weighed and homogenized in sterile PBS in ice. The tissue grinding solution was diluted from 10 to 10000 times with PBS. 100 μL tissue grinding solution was plated on the LB plate with 100 μg/ml ampicillin. The colonies formed after incubation for 12 h at 37℃ was counted.

4.9 In vivo tumor treatment

The 4T1 tumor-bearing mice with approximate tumor volume of 100 mm^3 were divided into 6 groups randomly (n = 6), including control group, ultrasound group, *E. coli* MG1655 group, URB group, ultrasound + *E. coli* MG1655 group and ultrasound + URB group. 1×10^7 URB was injected intravenously into tumor-bearing mice in URB group and ultrasound + URB group. 1×10^7 *E. coli* MG1655 was injected intravenously into tumor-bearing mice in *E. coli* MG1655 group and ultrasound + *E. coli* MG1655 group. The control group was injected with the same volume of saline. After 48 h of bacteria injection, the mice

in ultrasound group, ultrasound + *E. coli* MG1655 group and ultrasound + URB group were irradiated with the ultrasound for 30 min. The ultrasound parameter was as follows: acoustic pressure = 3.52 MPa, frequency = 960 Hz, pulse period = 150 ms, pulse width = 100 ms. During the irradiation, the infrared thermal imager was used to monitor the temperature change of the tumor site. The temperature of tumor tissue was stabilized at about 45℃ by adjusting the ON/OFF state of ultrasound (ON 10s, OFF 5s). The treatment procedure was performed day 0 and day 7. Then the mice weights and tumor volumes were recorded every 2 days. The calculation formula of tumor volume was: volume = ((tumor length) × (tumor width)^2)/2. When the mice died or the tumor volume exceeded 2000 mm^3, the death time was recorded to draw the survival curve. After the mice died, the tumor were collected and subjected to H&E staining, TUNEL assay and Ki67 staining.

For flow cytometry analysis of intratumoral immune cells, the tumors were collected at 7 days after treatments, cut into 1 mm^3 pieces and ground in the tissue grinder with cold PBS to obtain single cell suspension through a 70 μm strainer. The single cell suspension was blocked with CD16/32 antibodies, and then stained with fluorescent dye-conjugated antibody for 30 min at 4℃. For the analysis of macrophages, the single cell suspension was stained with CD11b-FITC, CD80-APC, CD86-PerCP-Cy5.5 and CD206-PE. For the analysis of T cells, the single cell suspension was stained with CD45-APC 750, CD3-APC, CD4-Alexa Flour 700 and CD8-FITC. For the analysis of DC, the cells were stained with CD45-APC 750, CD11c-PE, CD80-APC and CD86-PerCP-Cy5.5. For the analysis of NK cells, the cell was stained with CD45-APC 750, CD49-FITC. The samples were analyzed on a CytoFLEX flow cytometer (Beckman). The intratumor levels of IFN-γ, TNF-α and IL-10 were detected with ELISA kits (Dakewe) according to the test manual on the day 1, day 3, day 5 and day 7 after the treatment.

4.10 Distant tumor and metastasis treatment

For the 4T1 distant tumor model, 1 × 10^6 4T1 breast cancer cells were injected subcutaneously into the right flank of BALB/c female mice. On the third day after the inoculation, another 1 × 10^6 4T1 cells were injected into the left flank of mice. After 10 day of the first injection, the mice received 6 kinds of treatment (n = 6) as the same stated above. For the 4T1 tumor metastasis model, 1 × 10^6 4T1 breast cancer cells were injected subcutaneously into the right flank of BALB/c female mice. After 7 day of the injection, the mice received three kinds of treatment (n = 6) including control group, URB group and ultrasound + URB group. 1 × 10^7 URB was injected intravenously into tumor-bearing mice in URB group and ultrasound + URB group. The control group was injected with the same volume of saline. After 48 h of bacteria injection, the tumor of mice in ultrasound group and ultrasound + URB group were irradiated with the ultrasound for 30 min. The parameter of ultrasound was same as above. The treatment procedure was performed day 0 and day 7. The mice were euthanatized on the 21st day and the lung were collected in 4% paraformaldehyde. The number of metastatic nodules in the lungs was counted and the lung weight was measured. The lung slices were then stained with H&E to observe the metastasis foci. For flow cytometry analysis of spleen immune cells, the spleens were collected at 7 days after treatments, cut into 1 mm^3 pieces, and ground in the tissue grinder with cold PBS. The single cell suspension was obtained through a 70 μm strainer. The erythrocyte lysate was added to the cell suspension for 15 min

and centrifuged for 10 min to remove the RBC. The single cell suspension was analyzed by flow cytometer as stated above.

4.11 Biosafety assay

To evaluate the biosafety of URB, blood routine indexes, blood biochemical indexes and H&E staining were tested respectively. The female BALB/c mice were randomly divided into 3 groups (n = 5) including control group, URB group and ultrasound + URB group (dose of 1×10^7 CFU per mouse). The treated mice were sacrificed 2 days after ultrasound irradiation. Blood samples (0.8 mL for each mouse) were collected by eyeball extirpating. The organs were collected to perform H&E staining.

Declarations

Conflict of interest

The authors declare that there are no conflicts of interest.

Acknowledgments

This work was supported by National Key R&D Program of China [Grant Number 2020YFA0908800, 2019YFE0110400], Nationsal Natural Science Foundation of China [Grant Number 81971621, 81871376], and Natural Science Foundation of Guangdong Province [Grant Number 2021A1515011177, 2020A1515110628, 2019A1515012212 and 2018A030313678], Guangdong Innovation Platform of Translational Research for Cerebrovascular Diseases, and Shenzhen Science and Technology Innovation Committee [Grant Number. JCYJ20190812171820731 and JCYJ20180507182420114].

References

1. Lukasiewicz, K.; Fol, M., Microorganisms in the Treatment of Cancer: Advantages and Limitations. *Journal of Immunology Research* **2018**, 2018.
2. Mason, N. J.; Gnanandarajah, J. S.; Engiles, J. B.; Gray, F.; Laughlin, D.; Gaurnier-Hausser, A.; Wallecha, A.; Huebner, M.; Paterson, Y., Immunotherapy with a HER2-Targeting Listeria Induces HER2-Specific Immunity and Demonstrates Potential Therapeutic Effects in a Phase I Trial in Canine Osteosarcoma. *Clinical Cancer Research* 2016, *22* (17), 4380–4390.
3. Sang, W.; Zhang, Z.; Dai, Y. L.; Chen, X. Y., Recent advances in nanomaterial-based synergistic combination cancer immunotherapy. *Chemical Society Reviews* 2019, *48* (14), 3771–3810.
4. Yoon, W.; Park, Y. C.; Kim, J.; Chae, Y. S.; Byeon, J. H.; Min, S. H.; Park, S.; Yoo, Y.; Park, Y. K.; Kim, B. M., Application of genetically engineered Salmonella typhimurium for interferon-gamma-induced therapy against melanoma. *European Journal of Cancer* **2017**, *70*, 48–61.

5. Hernandez-Luna, M. A.; Luria-Perez, R., Cancer Immunotherapy: Priming the Host Immune Response with Live Attenuated Salmonella enterica. *Journal of Immunology Research* **2018**, 2018.
6. Huang, X. H.; Pan, J. M.; Xu, F. N.; Shao, B. F.; Wang, Y.; Guo, X.; Zhou, S. B., Bacteria-Based Cancer Immunotherapy. *Advanced Science* 2021, *8* (7).
7. Akin, D.; Sturgis, J.; Ragheb, K.; Sherman, D.; Burkholder, K.; Robinson, J. P.; Bhunia, A. K.; Mohammed, S.; Bashir, R., Bacteria-mediated delivery of nanoparticles and cargo into cells. *Nature Nanotechnology* 2007, *2* (7), 441–449.
8. Zheng, J. H.; Nguyen, V. H.; Jiang, S. N.; Park, S. H.; Tan, W.; Hong, S. H.; Shin, M. G.; Chung, I. J.; Hong, Y.; Bom, H. S.; Choy, H. E.; Lee, S. E.; Rhee, J. H.; Min, J. J., Two-step enhanced cancer immunotherapy with engineered Salmonella typhimurium secreting heterologous flagellin. *Science Translational Medicine* **2017**, *9* (376).
9. Nuyts, S.; Van Mellaert, L.; Theys, J.; Landuyt, W.; Bosmans, E.; Anne, J.; Lambin, P., Radio-responsive recA promoter significantly increases TNF alpha production in recombinant clostridia after 2 Gy irradiation. *Gene Therapy* 2001, *8* (15), 1197–1201.
10. Chowdhury, S.; Castro, S.; Coker, C.; Hinchliffe, T. E.; Arpaia, N.; Danino, T., Programmable bacteria induce durable tumor regression and systemic antitumor immunity. *Nature Medicine* **2019**, *25* (7), 1057-+.
11. Gurbatri, C. R.; Lia, I.; Vincent, R.; Coker, C.; Castro, S.; Treuting, P. M.; Hinchliffe, T. E.; Arpaia, N.; Danino, T., Engineered probiotics for local tumor delivery of checkpoint blockade nanobodies. *Science Translational Medicine* 2020, *12* (530).
12. Swofford, C. A.; Van Dessel, N.; Forbes, N. S., Quorum-sensing Salmonella selectively trigger protein expression within tumors. *Proceedings of the National Academy of Sciences of the United States of America* **2015**, *112* (11), 3457–3462.
13. Royo, J. L.; Becker, P. D.; Camacho, E. M.; Cebolla, A.; Link, C.; Santero, E.; Guzman, C. A., In vivo gene regulation in Salmonella spp. by a salicylate-dependent control circuit. *Nature Methods* 2007, *4* (11), 937–942.
14. Din, M. O.; Danino, T.; Prindle, A.; Skalak, M.; Selimkhanov, J.; Allen, K.; Julio, E.; Atolia, E.; Tsimring, L. S.; Bhatia, S. N.; Hasty, J., Synchronized cycles of bacterial lysis for in vivo delivery. *Nature* 2016, *536* (7614), 81-+.
15. Forbes, N. S., Engineering the perfect (bacterial) cancer therapy. *Nature Reviews Cancer* 2010, *10* (11), 784–793.
16. Wu, M. R.; Jusiak, B.; Lu, T. K., Engineering advanced cancer therapies with synthetic biology. *Nature Reviews Cancer* **2019**, *19* (4), 187–195.
17. Taylor, N. D.; Garruss, A. S.; Moretti, R.; Chan, S.; Arbing, M. A.; Cascio, D.; Rogers, J. K.; Isaacs, F. J.; Kosuri, S.; Baker, D.; Fields, S.; Church, G. M.; Raman, S., Engineering an allosteric transcription factor to respond to new ligands. *Nature Methods* 2016, *13* (2), 177-+.
18. Lagator, M.; Igler, C.; Moreno, A. B.; Guet, C. C.; Bollback, J. P., Epistatic Interactions in the Arabinose Cis-Regulatory Element. *Molecular Biology and Evolution* **2016**, *33* (3), 761–769.

19. Wen, M.; Zheng, J. H.; Choi, J. M.; Pei, J.; Li, C. H.; Li, S. Y.; Kim, I. Y.; Lim, S. H.; Jung, T. Y.; Moon, K. S.; Min, J. J.; Jung, S., Genetically-engineered Salmonella typhimurium expressing TIMP-2 as a therapeutic intervention in an orthotopic glioma mouse model. *Cancer Letters* 2018, *433*, 140–146.
20. Nuyts, S.; Van Mellaert, L.; Theys, J.; Landuyt, W.; Lambin, P.; Anne, J., The use of radiation-induced bacterial promoters in anaerobic conditions: A means to control gene expression in Clostridium-mediated therapy for cancer. *Radiation Research* 2001, *155* (5), 716–723.
21. Fan, J. X.; Li, Z. H.; Liu, X. H.; Zheng, D. W.; Chen, Y.; Zhang, X. Z., Bacteria-Mediated Tumor Therapy Utilizing Photothermally-Controlled TNF-alpha Expression via Oral Administration. *Nano Letters* 2018, *18* (4), 2373–2380.
22. Peek, M. C. L.; Ahmed, M.; Napoli, A.; ten Haken, B.; McWilliams, S.; Usiskin, S. I.; Pinder, S. E.; van Hemelrijck, M.; Douek, M., Systematic review of high-intensity focused ultrasound ablation in the treatment of breast cancer. *British Journal of Surgery* **2015**, *102* (8), 873–882.
23. Um, W.; Ko, H.; You, D. G.; Lim, S.; Kwak, G.; Shim, M. K.; Yang, S.; Lee, J.; Song, Y.; Kim, K.; Park, J. H., Necroptosis-Inducible Polymeric Nanobubbles for Enhanced Cancer Sonoimmunotherapy. *Advanced Materials* 2020, *32* (16).
24. Devarakonda, S. B.; Myers, M. R.; Lanier, M.; Dumoulin, C.; Banerjee, R. K., Assessment of Gold Nanoparticle-Mediated-Enhanced Hyperthermia Using MR-Guided High-Intensity Focused Ultrasound Ablation Procedure. *Nano Letters* **2017**, *17* (4), 2532–2538.
25. Liang, X. L.; Gao, J.; Jiang, L. D.; Luo, J. W.; Jing, L. J.; Li, X. D.; Jin, Y. S.; Dai, Z. F., Nanohybrid Liposomal Cerasomes with Good Physiological Stability and Rapid Temperature Responsiveness for High Intensity Focused Ultrasound Triggered Local Chemotherapy of Cancer. *Acs Nano* **2015**, *9* (2), 1280–1293.
26. Deng, Z. T.; Xiao, Y.; Pan, M.; Li, F.; Duan, W. L.; Meng, L.; Liu, X.; Yan, F.; Zheng, H. R., Hyperthermia-triggered drug delivery from iRGD-modified temperature-sensitive liposomes enhances the anti-tumor efficacy using high intensity focused ultrasound. *Journal of Controlled Release* 2016, *243*, 333–341.
27. Balbas, P.; Soberon, X.; Merino, E.; Zurita, M.; Lomeli, H.; Valle, F.; Flores, N.; Bolivar, F., PLASMID VECTOR PBR322 AND ITS SPECIAL-PURPOSE DERIVATIVES - A REVIEW. *Gene* **1986**, *50* (1–3), 3–40.
28. Zhang, C. L.; Qi, J. S.; Li, Y. J.; Fan, X. G.; Xu, Q. Y.; Chen, N.; Xie, X. X., Production of alpha-Ketobutyrate Using Engineered Escherichia coli Via Temperature Shift. *Biotechnology and Bioengineering* 2016, *113* (9), 2054–2059.
29. Ju, L. W.; Xing, L. H.; Hong, P. W.; Jin, W. J., GeneDn: for high-level expression design of heterologous genes in a prokaryotic system. *Bioinformatics* 1998, *14* (10), 884–885.
30. Schroder, K.; Hertzog, P. J.; Ravasi, T.; Hume, D. A., Interferon-gamma: an overview of signals, mechanisms and functions. *Journal of Leukocyte Biology* **2004**, *75* (2), 163–189.
31. Green, D. S.; Nunes, A. T.; Annunziata, C. M.; Zoon, K. C., Monocyte and interferon based therapy for the treatment of ovarian cancer. *Cytokine & Growth Factor Reviews* 2016, *29*, 109–115.
32. Garris, C. S.; Arlauckas, S. P.; Kohler, R. H.; Trefny, M. P.; Garren, S.; Piot, C.; Engblom, C.; Pfirschke, C.; Siwicki, M.; Gungabeesoon, J.; Freeman, G. J.; Warren, S. E.; Ong, S.; Browning, E.; Twitty, C. G.; Pierce,

R. H.; Le, M. H.; Algazi, A. P.; Daud, A. I.; Pai, S. I.; Zippelius, A.; Weissleder, R.; Pittet, M. J., Successful Anti-PD-1 Cancer Immunotherapy Requires T Cell-Dendritic Cell Crosstalk Involving the Cytokines IFN-gamma and IL-12. *Immunity* 2018, *49* (6), 1148-+.

33. Sonntag, L.; Simmchen, J.; Magdanz, V., Nano-and Micromotors Designed for Cancer Therapy. *Molecules* 2019, *24* (18).
34. Xie, S. Z.; Zhao, L.; Song, X. J.; Tang, M. S.; Mo, C. F.; Li, X. H., Doxorubicin-conjugated Escherichia coli Nissle 1917 swimmers to achieve tumor targeting and responsive drug release. *Journal of Controlled Release* 2017, *268*, 390–399.
35. Chen, W. F.; Wang, Y.; Qin, M.; Zhang, X. D.; Zhang, Z. R.; Sun, X.; Gu, Z., Bacteria-Driven Hypoxia Targeting for Combined Biotherapy and Photothermal Therapy. *Acs Nano* 2018, *12* (6), 5995–6005.
36. Zheng, D. W.; Chen, Y.; Li, Z. H.; Xu, L.; Li, C. X.; Li, B.; Fan, J. X.; Cheng, S. X.; Zhang, X. Z., Optically-controlled bacterial metabolite for cancer therapy. *Nature Communications* 2018, *9*.
37. Zhu, C. L.; Yang, Q.; Lv, F. T.; Liu, L. B.; Wang, S., Conjugated Polymer-Coated Bacteria for Multimodal Intracellular and Extracellular Anticancer Activity. *Advanced Materials* 2013, *25* (8), 1203–1208.
38. Baer, C.; Squadrito, M. L.; Laoui, D.; Thompson, D.; Hansen, S. K.; Kiialainen, A.; Hoves, S.; Ries, C. H.; Ooi, C. H.; De Palma, M., Suppression of microRNA activity amplifies IFN-gamma-induced macrophage activation and promotes anti-tumour immunity. *Nature Cell Biology* 2016, *18* (7), 790-+.
39. Alspach, E.; Lussier, D. M.; Schreiber, R. D., Interferon gamma and Its Important Roles in Promoting and Inhibiting Spontaneous and Therapeutic Cancer Immunity. *Cold Spring Harbor Perspectives in Biology* 2019, *11* (3).
40. Zhang, M. J.; Huang, L. F.; Ding, G. P.; Huang, H. L.; Cao, G. L.; Sun, X.; Lou, N.; Wei, Q.; Shen, T.; Xu, X. D.; Cao, L. P.; Yan, Q., Interferon gamma inhibits CXCL8-CXCR2 axis mediated tumor-associated macrophages tumor trafficking and enhances anti-PD1 efficacy in pancreatic cancer. *Journal for Immunotherapy of Cancer* **2020**, *8* (1).
41. Xu, H. N.; Jiang, Y.; Xu, X. Q.; Su, X. P.; Liu, Y.; Ma, Y. W.; Zhao, Y.; Shen, Z. Y.; Huang, B.; Cao, X. T., Inducible degradation of lncRNA Sros1 promotes IFN-gamma-mediated activation of innate immune responses by stabilizing Stat1 mRNA (vol 20, pg 1621, 2019). *Nature Immunology* **2020**, *21* (4), 477–478.
42. Xin, G.; Schauder, D. M.; Jing, W. Q.; Jiang, A. M.; Joshi, N. S.; Johnson, B.; Cui, W. G., Pathogen boosted adoptive cell transfer immunotherapy to treat solid tumors. *Proceedings of the National Academy of Sciences of the United States of America* **2017**, *114* (4), 740–745.
43. Rodell, C. B.; Arlauckas, S. P.; Cuccarese, M. F.; Garris, C. S.; Ahmed, R.; Kohler, R. H.; Pittet, M. J.; Weissleder, R., TLR7/8-agonist-loaded nanoparticles promote the polarization of tumour-associated macrophages to enhance cancer immunotherapy. *Nature Biomedical Engineering* 2018, *2* (8), 578–588.

Figures

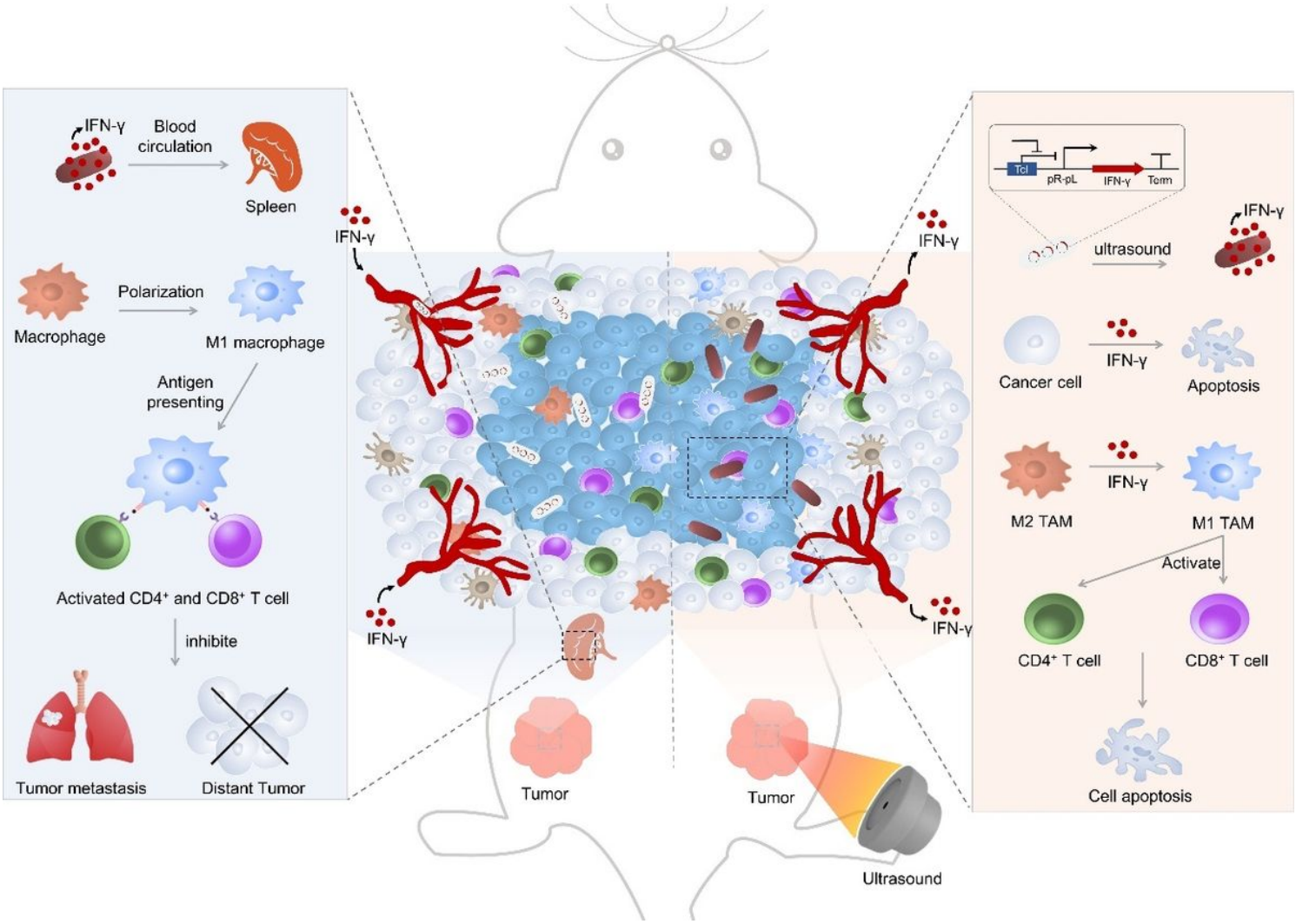

Figure 1

Schematic diagram of URB in controlling IFN-γ expression by focused ultrasound and their mechanisms for cancer immunotherapy.

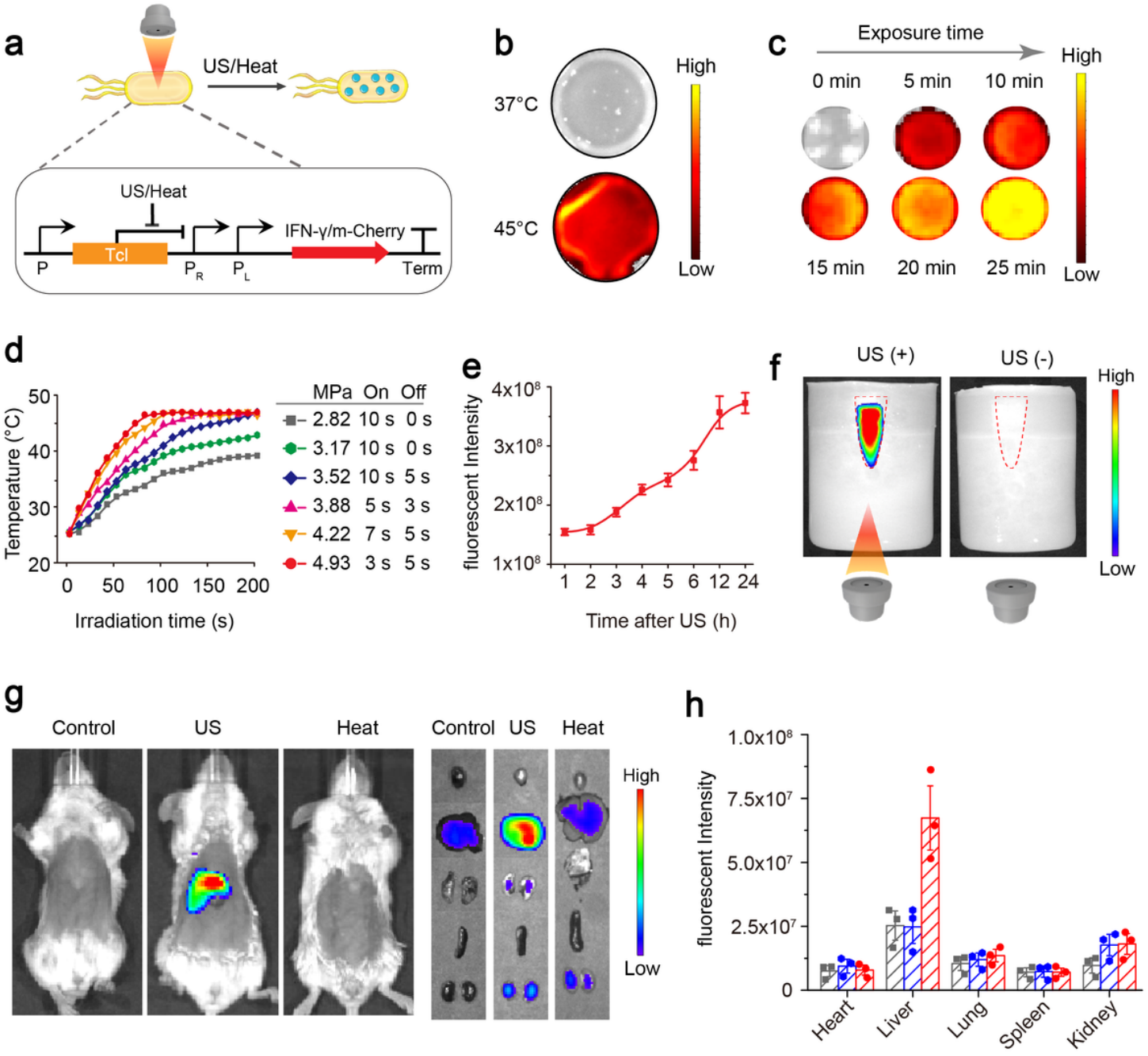

Figure 2

The gene expression of URB trigged by hyperthermia and ultrasound. a: Mechanism of mCherry/IFN-γ expression based on pBV220 plasmid in the bacteria. b: Fluorescence image of mCherry protein in URB under different temperature. c: Fluorescence image of mCherry protein in URB under 45 °C with different time. d: Quantification of temperature of bacteria solution irradiated with the different acoustic pressures by focused ultrasound. e: Quantification of fluorescence signals of bacteria solution after ultrasound irradiation. f: Fluorescence image of mCherry protein of URB in the center of the gel phantom under ultrasound irradiation. g: Fluorescence image of mice injected with 1 × 107 CFU of URB under liver-

targeted ultrasound irradiation. h: Quantification of fluorescence signals of major organs of mice injected with 1 × 107 CFU of URB under liver-targeted ultrasound irradiation.

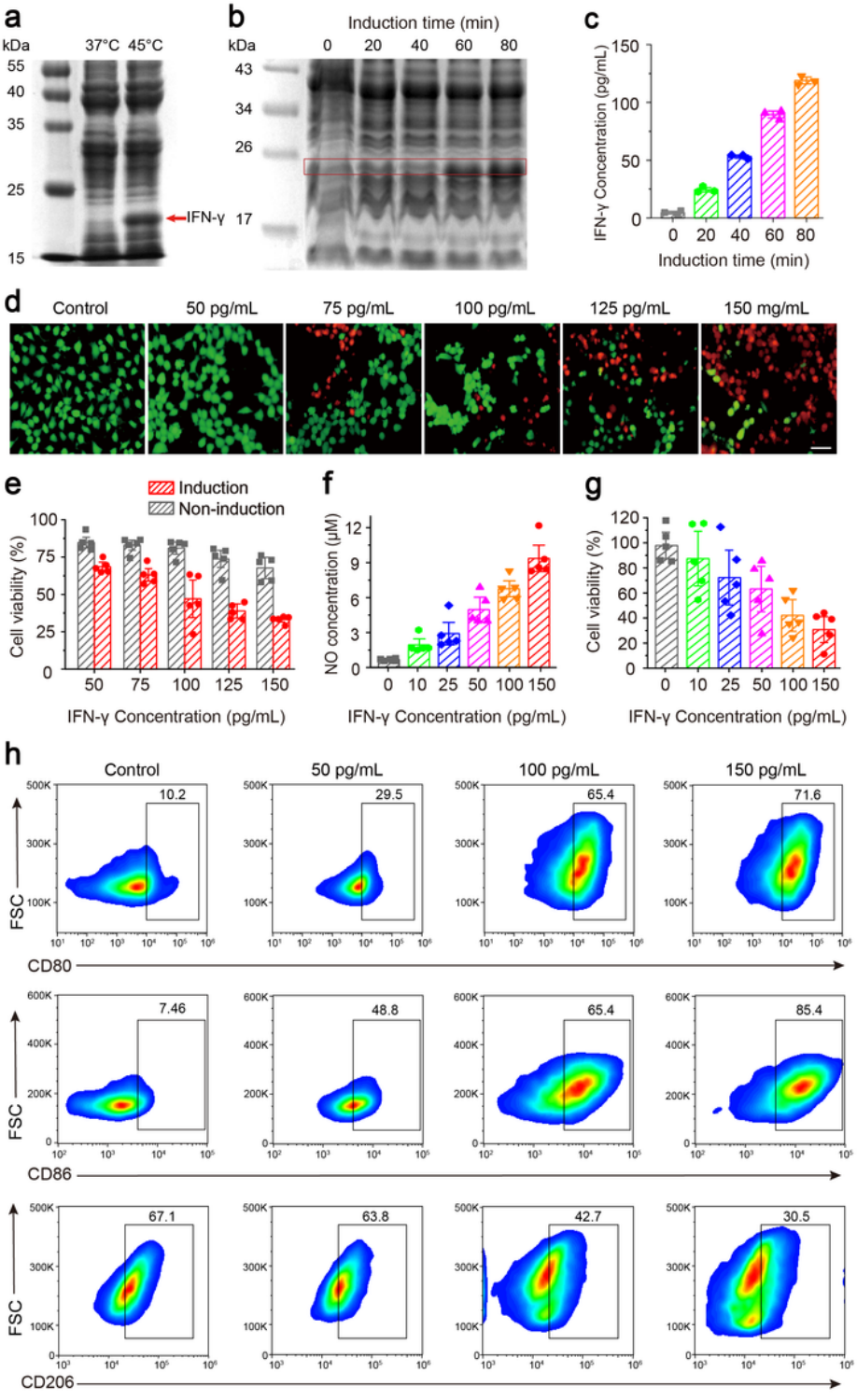

Figure 3

In vitro characterization of URB. a: Representative SDS-PAGE image of IFN-γ protein expressed in URB under different temperature. b: Representative SDS-PAGE image of IFN-γ protein expressed in URB under 45°C with different time. c: Quantitative analysis of IFN-γ protein content in bacterial culture medium

under ultrasound irradiation with different time. d: Fluorescence microscopy image of breast cancer cells stained with Calcein-AM and PI after different IFN-γ levels bacterial culture medium treatment (scale bar = 20 μm). e: Viability assay of cells treated with bacterial culture medium with different IFN-γ concentrations. f: Quantitative analysis of NO concentrations in the cell culture medium of macrophages RAW 264.7 treated with different bacterial IFN-γ concentrations. g: Cytotoxicity of macrophages stimulated with different IFN-γ concentrations to breast cancer cells. MOI ratio = 5:1 (tumor cells: macrophages). h: Flow cytometry analysis of M1 phenotype macrophages (CD80+/CD86+) and M2 phenotype macrophages (CD206+) after different IFN-γ levels bacterial culture medium treatment.

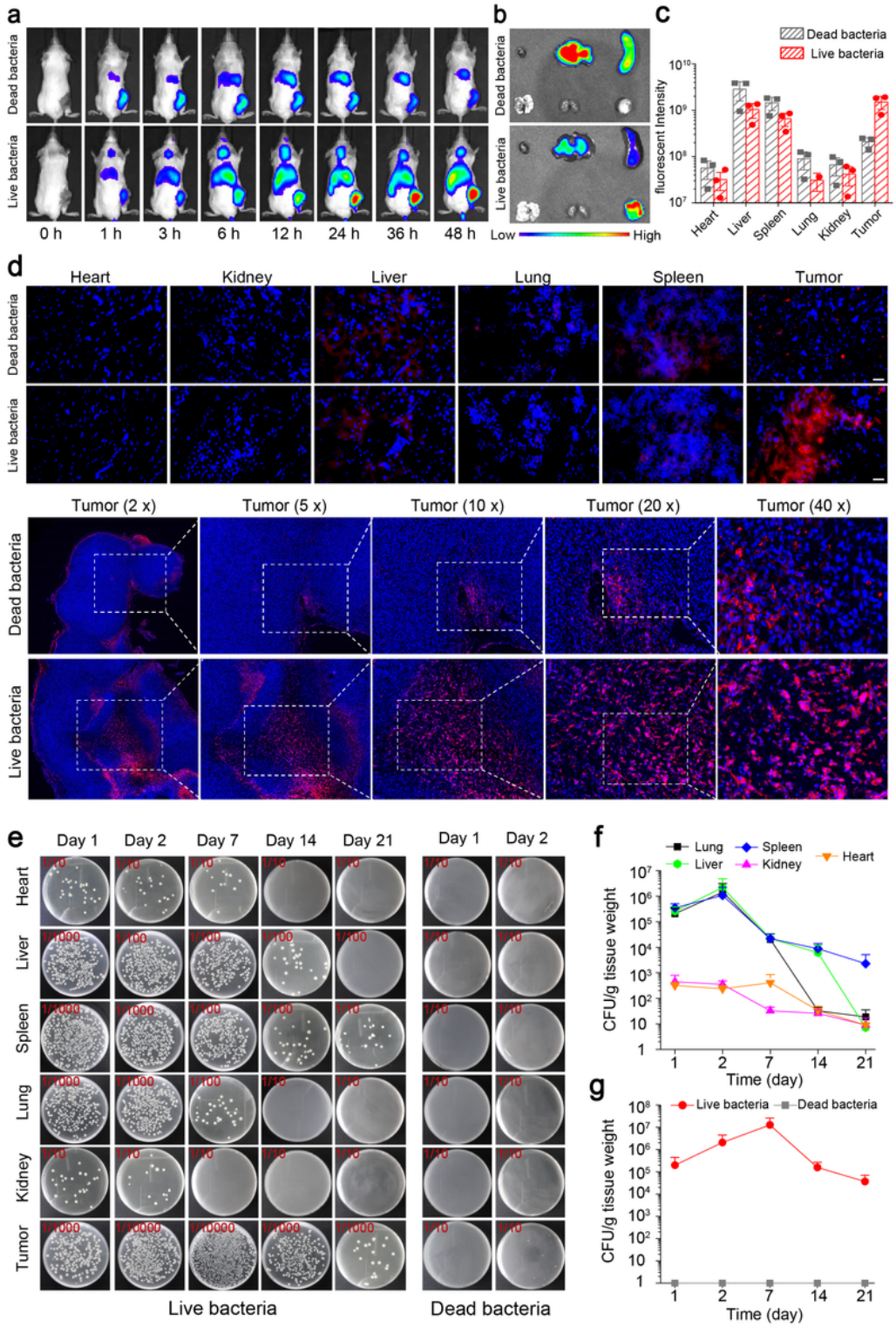

Figure 4

Tumor targeting of URB. a: In vivo fluorescence imaging of tumor-bearing mice different time after intravenous injection of 1 × 107 CFU of DiR-stained live URB or heating-inactivated bacteria. b, c: The intensities of fluorescence imaging (b) and corresponding fluorescence signal of tumor and major organs of tumor-bearing mice 48 h after intravenous injection of 1 × 107 CFU of DiR-stained live URB or heating-inactivated bacteria. d: Fluorescence microscopy image of tumor and major organs of tumor-bearing

mice 48 h after intravenous injection of 1 × 107 CFU of DiR-stained URB (scale bar=25 μm). e: Photographs of solid LB agar plates of bacterial colonization in tumor and major organs collected from tumor-bearing mice at different time points after intravenous administration of 1 × 107 CFU of URB. f, g: Quantification of bacterial colonization in major organs(f) and tumor(g) collected from tumor-bearing mice at different time points after administration of 1 × 107 CFU of URB.

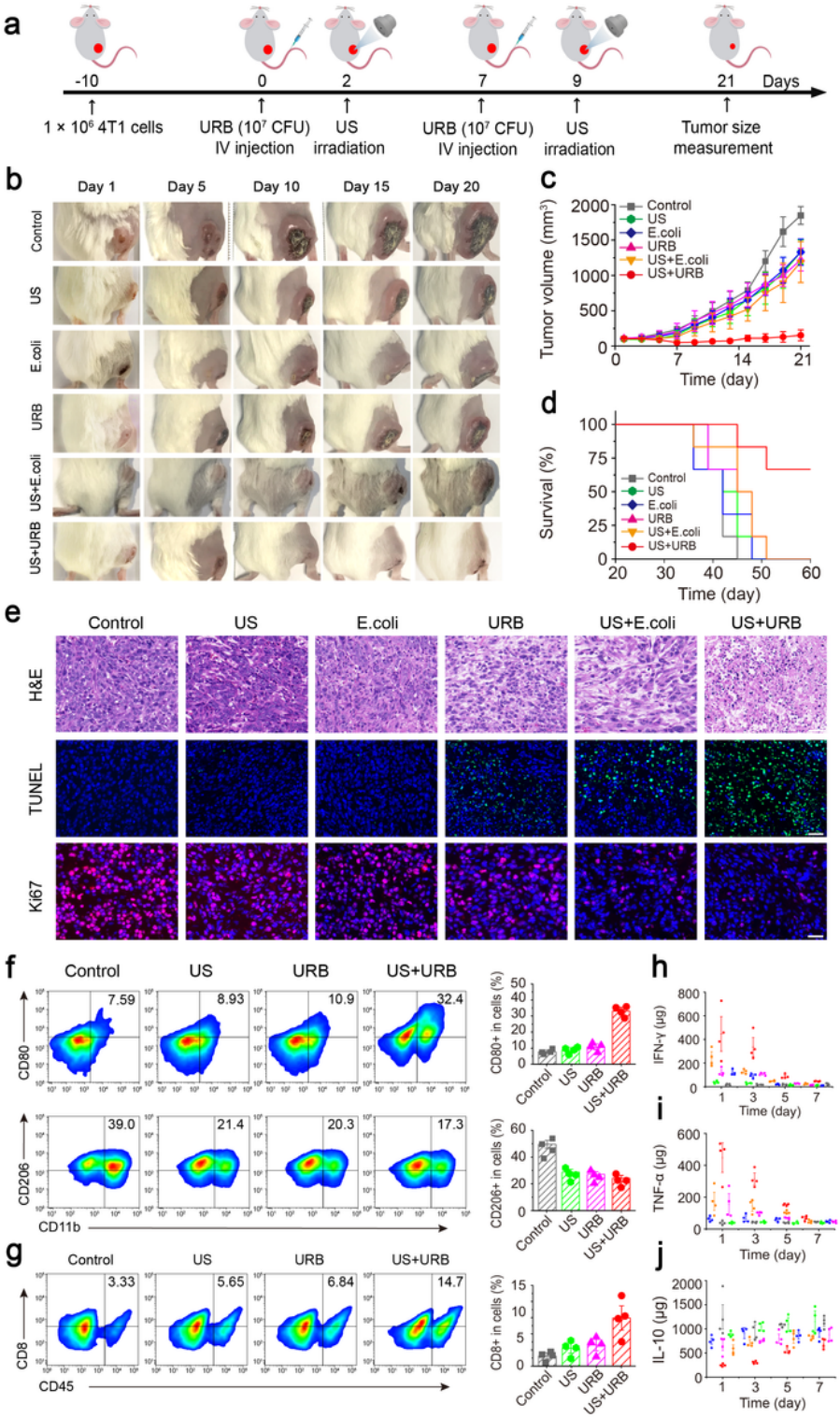

Figure 5

URB-mediated tumor immunotherapy. a: Schematic illustration of URB-mediated tumor immunotherapy to inhibit tumor growth in a 4T1 subcutaneous tumor transplantation mouse model. b: Representative tumor photographs of the tumor-bearing mice after different treatments. c: Tumor growth curve of tumor-bearing mice treated with different treatments. d: Survival curves for different treatment groups. e: H&E-stained, TUNEL-stained and Ki-67-stained tumor slices for each group (Scale bar=100 μm). f: Flow cytometric analysis and quantification of M1 macrophages (CD80+CD11b+) and M2 macrophages (CD206+ CD11b+) in tumor. g: Flow cytometric analysis and quantification of CD8+ T cell (CD8+CD45+) in tumor. h-j: IFN-γ, TNF-α and IL-10 levels in tumors at 1, 3, 5, 7 days after different treatments. Data are presented as mean ± S.D. Statistical analysis was calculated by using one-way analysis of variance with a Tukey's test (***P < 0.001; **P < 0.01; *P < 0.05;).

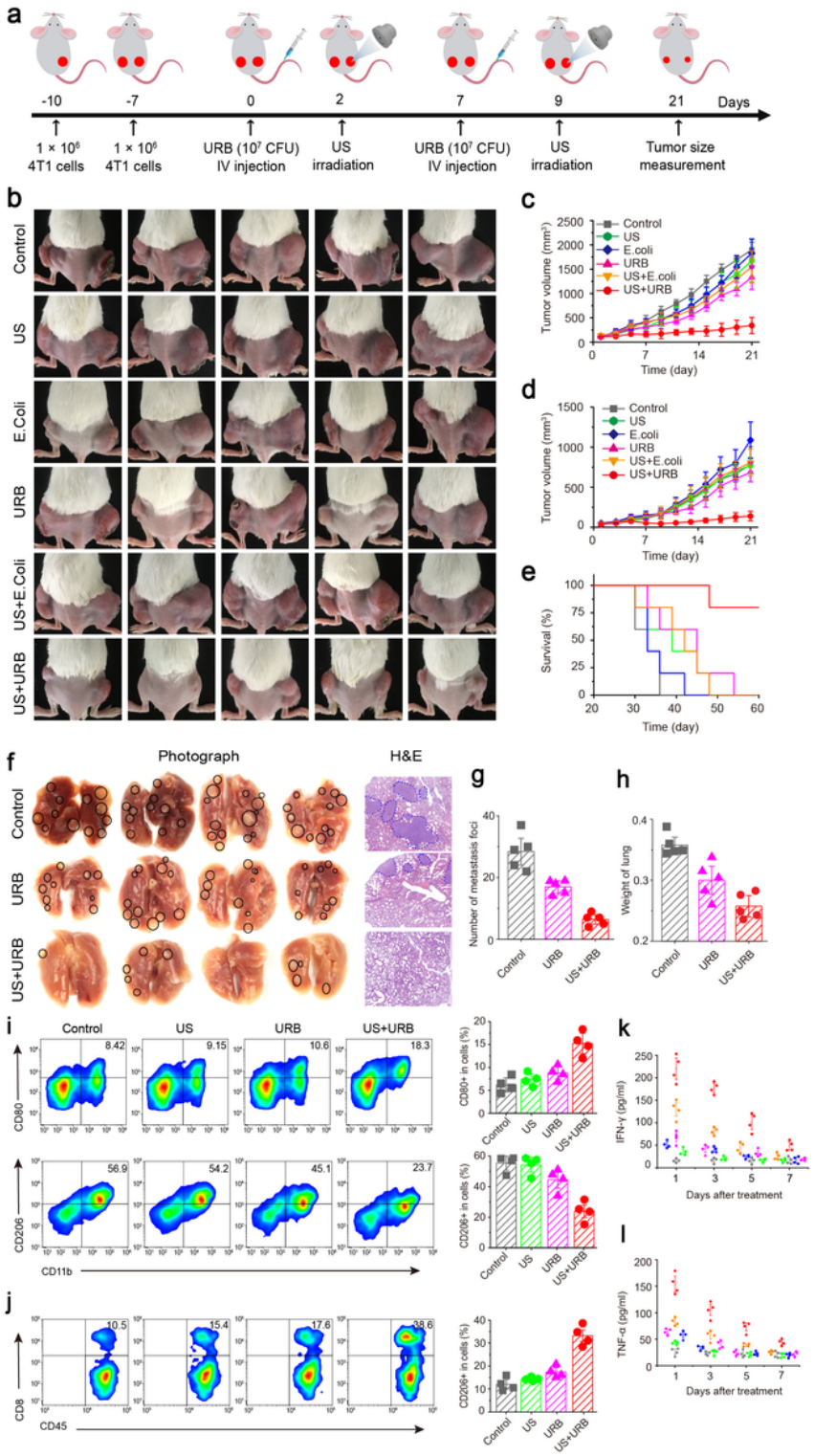

Figure 6

URB inhibited distant tumor growth and metastasis. a: Schematic showing the treatment mode in a distant tumor mouse model. b: Representative tumor photographs of distant tumor treatment in different groups. c: Primary tumor growth curve of mice treated with different treatments. d: Distant tumor growth curve of mice treated with different treatments. e: Survival curves for different treatment groups. f: Photographs of Lung and corresponding H&E-stained lung slices collected from the different group mice

after treatment. g: Count of metastasis foci in the lung of different groups. h: The weight of the lung of different groups. i: Flow cytometric analysis and quantification of M1 macrophages (CD80+CD11b+) and M2 macrophages (CD206+ CD11b+) in spleen. j: Flow cytometry analysis and quantification of CD8+ T cell (CD8+CD45+) in spleen. k,l: IFN-γ and TNF-α levels in blood from mice at 1, 3, 5, 7 days after different treatments. Data are presented as mean ± S.D. Statistical analysis was calculated by using one-way analysis of variance with a Tukey's test (***P < 0.001; **P < 0.01; *P < 0.05;).

Supplementary Files

This is a list of supplementary files associated with this preprint. Click to download.

- Supplementaryinformation.docx